Formation of plasmoids during sawtooth crashes

Q. Yu, S. Günter and K. Lackner

Max-Planck/Princeton Center for Plasma Physics and

Max-Planck-Institut für Plasmaphysik, 85748 Garching, Germany

The nonlinear growth of the internal kink mode is studied numerically using reduced MHD equations in cylinder geometry. For low Lundquist numbers, $S<10^7$, the already well known results have been reproduced: a m/n=1/1 magnetic island (m: poloidal, n: toroidal mode number) grows while the original core shrinks until full reconnection is achieved. For higher S values, however, the dynamics is found to be qualitatively different from the well-known Kadomtsev's model (B. B. Kadomtsev, Sov. J. Plasma Phys. **1** (1975) 389). The growth of the 1/1 island causes the development of a very thin current sheet which becomes tearing unstable. The current sheet is thus broken up and secondary islands (plasmoids) form. These plasmoids strongly speed up the reconnection and eventually coalesce into one secondary island. The formation of a large secondary island stops the fast reconnection process, leading even to a partial reversal of this process. The final state of sawtooth reconnection is thus no longer an axis-symmetric equilibrium as in case of complete reconnection for low S value, but a helical equilibrium with two coexisting magnetic islands.

1. Introduction

Magnetic reconnection is a fundamental plasma phenomenon observed, e.g., in solar flares, magnetotail and fusion devices. Common to all these reconnection phenomena in such low collisionality plasmas is that a simple MHD description leads to reconnection times orders of magnitude longer than the observed time scales. This is also true for the fast reconnection events typical for tokamak plasmas, the sawteeth [1].

Sawteeth are quasi-periodic events, that flatten the plasma pressure profile inside the q=1 surface on a very short time scale due to fast growing magnetic island caused by the m/n=1/1 internal kink mode [2] (q being the safety factor, and m and n the poloidal and toroidal mode numbers, respectively). Large amplitude sawtooth crashes are able to even trigger additional instabilities such as neoclassical tearing modes (NTMs) that degrade the plasma confinement also outside the q=1 surface.

Since their first discovery [l], sawtooth instabilities have attracted much research interest [2-23]. Using a Sweet-Parker type analysis [24,25], the sawtooth crash time has been found by Kadomtsev to be about $(\tau_A\tau_R)^{1/2}$, where τ_A is the Alfúen time, and τ_R is the resistive time [2]. While the sawtooth crash times observed in small tokamaks with quite resistive plasmas can be explained by the Kadomtsev model [2], experimental measurements in high temperature tokamak plasmas resulted in crash times of the order of 100 μs [3-5], being much shorter than predicted by Kadomtsev. Therefore, several extensions of the theoretical model beyond resistive MHD have been considered, including the electron inertia effect [6], anomalous current diffusion [7-l0], finite ion Larmor radius [12, 14-16] and the parallel electron viscosity [17], to understand the fast growth of the m/n=1/1 island.

Besides the reconnection rates, some other observations are often in contradiction with theoretical results. For example, partial reconnection is often observed in

experiments [19], while resistive MHD simulations so far always lead to full reconnection.

In this paper, reduced MHD simulations for sawtooth crashes are performed with Lundquist numbers S up to values as characteristic for high-temperature tokamak plasmas. It will be shown that the dynamics for low and high S numbers differ significantly. For high S numbers very thin current sheets occur that become tearing unstable. The current sheets are thus broken up and secondary islands form. These islands finally coalesce into one secondary island. A sufficiently large secondary island eventually stops the fast reconnection process, leading even to a partial reversal of this process. The final state of sawtooth reconnection is thus no longer an axis-symmetric equilibrium as in case of complete reconnection for low S number, but a helical equilibrium with two coexisting magnetic islands.

2. Theoretical model and numerical results

The large aspect-ratio tokamak approximation is used for our simulations. The magnetic field is defined as $\mathbf{B}=B_{0t}(\mathbf{e}_t-\mathbf{e}_\theta k_t/k_\theta)+\nabla\psi\times\mathbf{e}_t$, where ψ is the helical flux function, $k_\theta=m/r$ and $k_t=n/R$ are the wave vectors in $\mathbf{e}_\theta$ (poloidal) and $\mathbf{e}_t$ (toroidal) direction, r and R are the minor and the major radius, and the subscript 0 denotes an equilibrium quantity. The plasma velocity is given by $\mathbf{v}=\nabla\phi\times\mathbf{e}_t$, where ϕ is the stream function.

Ohm's law and the equation of motion in the perpendicular direction (after taking $\mathbf{e}_t\cdot\nabla\times$) are solved. Normalizing the length to the minor radius a, the time t to the resistive time $\tau_R=a^2\mu_0/\eta$ (η is the plasma resistivity), the helical flux ψ to aB_{0t}, and $\mathbf{v}$ to a/τ_R, these equations become [28]

$$\frac{d\psi}{dt} = E_0 - \eta j - \frac{\eta}{\nu_{ei}} \mu_e \nabla_\perp^2 j , \quad (1)$$

$$\frac{dU}{dt} = -S^2 \nabla_\parallel j + \mu \nabla_\perp^2 U , \quad (2)$$

where $d/dt = \partial/\partial t + \boldsymbol{v}_\perp \cdot \nabla_\perp$, $j = -\nabla_\perp^2 \psi - 2nB_0/(mR)$ is the parallel plasma current density, and $U = -\nabla_\perp^2 \phi$ is the plasma vorticity. $\tau_A = a/V_A$ is the Alfvén time, V_A is defined using the toroidal field, and η is the normalized resistivity. E_0 denotes the equilibrium electric field, μ the normalized ion viscosity, μ_e the perpendicular electron viscosity, and υ_{ei} is the electron-ion collisional frequency. A constant plasma resistivity over the whole plasma is assumed. The last term in equations (1) and (2) corresponds to the perpendicular electron and ion viscosity, included for improved numerical stability only.

Equations (1) and (2) are solved by using the initial value code TM1, which has been used for modelling the nonlinear growth of tearing modes and the plasma response to RMPs earlier [26-28]. Extensive numerical calculations have been carried out using different q-profiles and S values. In order to ensure numerical convergence, the radial grid size is taken to be in the range $(2.0\text{-}6.3)\times 10^{-4}$a, and tens of Fourier components are included in calculations. A finite perpendicular electron viscosity improves the numerical convergence, while it does not significantly affect the results if chosen not too large. For lower S values, $S<10^7$, as reported from earlier simulations [e.g. 18], a growing m/n=1/1 island is found, which finally occupies the whole region inside the q<1 surface. Meanwhile, the original core shrinks and eventually disappears. For higher S values the reconnection proceeds in a qualitatively different form. To demonstrate this, constant-ψ contours are shown in the R-Z plane in figure 1 for $S=2.65\times 10^7$ at different times, where R=0 corresponds to the major radius of the original magnetic axis, and Z is the coordinate along the vertical direction, normalized to the plasma minor radius a. As the starting point for these simulations, a monotonic q-profile is assumed with the q=1

surface located at r_s=0.3a, and $q_{(r=0)}$=0.9 at the original magnetic axis. In the simulations $\mu=18.8(a^2/\tau_R)$ and $\mu_e/\upsilon_{ei} = 10^{-4}a^2$ are used. After an initial growth phase of the m=1 mode a thin current layer develops at the X-point region, which becomes tearing unstable, leading to a break-up into 1 or several islands (figure 1a). The number of "secondary" islands generated increases with the S-number, concomitant with a narrowing of the current layer (figure 2). Subsequently, however, these secondary islands coalesce again to a single one independently from S. The further growth of this secondary island leads to a squeezing of the original core, with "tertiary" islands tearing off and migrating into the outer plasma zone (figure 1b). They convect with them plasma and toroidal flux from the original core region and deposit it in the region q >1. The tertiary islands dissolve there, obviously because their radial squeezing by the ambient field increases strongly (for a given trapped helical flux) the local current density and hence the rate of resistive flux annihilation. After this loss of plasma and toroidal flux the original core assumes again a more circular shape (figure 1c), and the reconnection process actually reverses. Ultimately a resistively stable helical state established, which changes only on the global current diffusion time within the q=1 surface (figure 1d). For the final state, using field line tracing, the q value at the magnetic axis is found to be about the same as its original value before mode growth, as expected.

Fig. 2 shows contours of the current density for different S values right after the current sheet became tearing unstable: $S=2.65\times10^7$ in figure 2(a), 2.65×10^8 in 2(b) and 2.65×10^9 in 2(c), respectively. For the lowest S number, one finds the formation of a single secondary island (the current sheet is broken into two parts only, as shown in Fig. 2a). For higher S values, $S=2.65\times10^8$ and 2.65×10^9, multiple secondary islands form. No matter how many small secondary islands appear at the beginning, however, only one secondary island grows to large amplitude as shown in figure 1. For higher S values, the

current sheet becomes tearing unstable already earlier in the reconnection process, i.e. for a smaller 1/1 island. Figure 2d shows the plasma current density in the late nonlinear phase for $S=2.65\times10^7$. In this phase the contours of the current density are similar to that of the helical flux, indicating that the current density is essentially a function of the helical flux. This corresponds to the Rutherford regime of the m>1 tearing mode [29], being consistent with the slow change of the island in this phase.

Figure 3a shows the time evolution of the helical flux at the x- point, ψ_x, (solid curve with circles) and the o-point, ψ_o, (dotted curve) of the m/n=1/1 island for several values of S. The dashed curves correspond to the helical flux at the o-point of the secondary island. During the reconnection process, ψ_x decreases in time while ψ_o changes little, as expected. For low S numbers ($S<10^7$), full reconnection occurs without the occurrence of secondary islands. For $S>10^7$, a secondary island grows as indicated by the dashed curve, and its growth rate is about the same as that of the 1/1 island during its growing phase. Increasing the S value, the amount of reconnected flux decreases, corresponding to smaller saturated 1/1 island width (see figure 4), and the secondary island forms already at a smaller reconnected flux. For intermediate S values ($10^7\leq S<10^8$), the reconnection process reverses to some extent after the formation of the secondary island. The secondary island prevents fast full reconnection for $S>10^7$.

Figure 3(b) is similar to 3(a) except that the helical flux at the x- point (marked as x-3rd) and the o-point (marked as o-3rd) of the third island (as indicated in Fig. 1b) is shown as a function of time for $S=2.65\times10^7$. The small difference between the helical flux at these two points is consistent with the small island size seen in figures 1b and 1c. The third island only exists for a short time period. It also appears for $S=2.65\times10^8$, but vanishes for $S\geq10^9$. The reason is probably the smaller saturated width of the 1/1 island that prevents the squeezing of the original plasma core.

The maximum ($S<10^9$) or saturated ($S\geq10^9$) radial island width during the island growth, is shown in figure 4 as function of S. For $S<10^7$, only the m/n=1/1 island appears with a maximum radial width somewhat larger than twice the original q=1 radius ($2r_s=0.6a$). The q=1 radius of the final state is larger than the original one due to the modification of the plasma current density profiles by the island. For $S \geq10^7$, a secondary island forms. For $S\geq10^9$, the saturated widths of the 1/1 island is significantly smaller than that for lower S values.

The reconnection time is shown in figure 5 as function of S. The curve with circles shows the growth time of the m/n=1/1 island from an initial width of W=0.1a up to the maximum ($S<10^9$) or saturated ($S\geq10^9$) island width. The straight line with triangles is the reconnection time calculated from Kadomtsev's model. The reconnection time agrees with Kadomtsev's model for $S<10^7$ but is much shorter for larger S values. For these S values, the formation of secondary islands accelerates the reconnection process significantly.

3. Discussion and summary

In this paper, it is shown that at high S number the nonlinear development of the 1/1 instability becomes qualitatively different, and the scaling of reconnection rate deviates from the Kadomtsev model. Rather than proceeding to full reconnection, a very thin current sheet forms around the X-point of the 1/1 island that becomes tearing unstable and gives rise to the formation of secondary islands (plasmoids). Such a result is consistent with both the analytical linear theory and numerical calculations on magnetic reconnection in slab geometry, which show that a thin plasma current sheet could be unstable to the tearing mode and broken up [e.g. 30-33]. The formation of these plasmoids accelerates the reconnection (see Fig.5). The number of higher order islands

formed during the early reconnection phase increases with the S number. On a longer time scale, only one secondary island grows into a large size. This island stops the fast reconnection process and even slightly reverses it, ultimately leading to a quasi-stationary state. The latter persists on a long time scale, characteristic for the current re-arrangement within the q=1 surface, or the sawtooth period. It is characterized by a persistent 2/2 component of the perturbation, which is also experimentally observed in many cases [19,20]. In particular this would offer also an explanation for the triggering of m/n=3/2 neoclassical tearing modes by sawteeth, which is difficult to explain by the action of a short perturbation only during the sawtooth crash phase. It has been shown in experiments that the m/n=3/2 NTM seeding could be due to the precursor to the sawtooth [34]. An example of plasmoids formation during resistive kink mode growth was already shown before [35], possibly triggered by an additional tearing-like perturbation, since the helical flux contour becomes up-down asymmetry in the later phase.

The presented results are very robust. Secondary islands are always observed independent of the initial q-profiles if the S value is sufficiently high. The results are also independent on the perpendicular electron viscosity or ion viscosity. The critical aspect ratio of the current sheet (ratio between its poloidal and radial extent, calculated from the half width of the current density perturbation around the x-point) is found to be about 60. Above that value we find the formation of secondary islands for $S=10^7$.

The simulation results presented here are restricted to resistive MHD, and hence do not include two-fluid effects, such as the parallel electron pressure gradient (diamagnetic drift) and electron inertia [7-17,36]. Those effects might significantly affect the results presented in this paper. Magnetic islands generated by electron temperature gradient or plasma turbulence could also have an effect [27,37,38]. These results remain, however, im-

portant within the resistive MHD picture as a qualitative correction to previous simulations at (unrealistic) lower S numbers. The well-known Kadmotsev's model is only applicable for low S values ($S<10^7$).

Acknowledgement: The authors would like to thank A. Bhattacharjee for valuable discussions.

REFERENCES

[1] S. Von Goeler *et al*., Phys. Rev. Lett. **33** (1974) 1201.

[2] B. B. Kadomtsev, Sov. J. Plasma Phys. **1** (1975) 389.

[3] A. W. Edwards *et al*., Phys. Rev. Lett. **57** (1986) 210.

[4] L. McGuire, TFTR Group, Phys. Fluids **B 2** (1990) 1287.

[5] J. A. Wesson *et al*., Nucl. Fusion **31** (1990) 111.

[6] J. A. Wesson, Nucl. Fusion **30** (1990) 2545.

[7] J. F. Drake and R. G. Kleva, Phys. Rev. Lett. **66** (1991) 1458.

[8] M. Ottaviani and F. Porcelli, Phys. Rev. Lett. **71** (1993) 3802.

[9] D. Biskamp and J. F. Drake, Phys. Rev. Lett. **73** (1994) 97 1.

[10] J. F. Drake *et al*., Phys. Rev. Lett. **73** (1994) 1251.

[11] F. Waelbroeck, Phys. Fluids **B 1** (1989) 2372.

[12] L. E. Zakharov *et al*., Phys. Fluids **B 5** (1993) 2498.

[13] D. Biskamp, Phys. Fluids **B 3** (1991) 3353.

[14] X. Wang and A. Bhattarchajee, Phys. Rev. Lett. **70** (1993) 1627.

[15] F. Porcelli, Phys. Rev. Lett. **66** (1991) 425.

[16] A. Y. Aydemir, Phys. Fluids **B 4** (1992) 3469.

[17] Qingquan Yu, Nucl. Fusion **35** (1995) 1012.

[18] A. Skyes and J. A. Wesson, Phys. Rev. Lett. **37** (1976) 140.

[19] V. Igochine, J. Boom, I. Classen *et al*., Phys. Plasmas **17**, 122506 (2010).

[20] X. Xu, J. Wang, Y. Wen *et al*., Plasma Phys. Control. Fusion, **52**, 015008 (2010).

[21] F. Porcelli, D. Boucher and M. N. Rosenbluth, Plasma Phys. Control. Fusion, **38**, 2163 (1996).

[22] F. D. Halpern, D. Leblond, H. Lütjens and J-F Luciani, Plasma Phys. Control. Fusion, **53**, 015001 (2011).

[23] F. D. Halpern, H. Lütjens and J-F Luciani, Phys. Plasmas **18**, 102501 (2011).

[24] P. A. Sweet, in Electromagnetic Phenomena in Cosmic Physics (B. Lehnert Ed.), Cambridge University Press, Cambridge (1958) 123.

[25] E. N. Parker, J. Geophys. Res. **62** (1957) 509.

[26] Q. Yu, S. Günter and and K. Lackner, Phys. Plasmas **11**, 140 (2004).

[27] Q. Yu, Nucl. Fusion **50**, 025014 (2010).

[28] Q. Yu and S. Günter, Nucl. Fusion **49**, 062001 (2009).

[29] P. H. Rutherford, Phys. Fluids **16**, 1903 (1973).

[30] H. P. Furth, J. Killeen, and M. N. Rosenbluth, Phys. Fluids **6**, 456 (1963).

[31] Yi-Min Huang, A. Bhattacharjee, and Brian P. Sullivan, Phys. Plasmas **18**, 072109 (2011)

[32] N. F. Loureiro, A. A. Schekochihin and S. C. Cowley, Phys. Plasmas **14**, 100703 (2007)

[33] S. Schmidt, S. Günter and K. Lackner, Phys. Plasmas **16**, 072302 (2009)

[34] R. J. Buttery, T. C. Hender, D. F. Howell, R. J. La Hay *et al*., Nucl. Fusion **43**, 69 (2003)

[35] D. Biskamp, Phys. Fluids **29**, 1520 (1986)

[36] D. Biskamp and T. Sato, Phys. Plasmas **4**, 1326 (1997)),

[37] A. Ishizawa and N. Nakajima, Phys. Plasmas **14**, 040702 (2007)).

[38] A. Ishizawa and N. Nakajima, Phys. Plasmas **17**, 072308 (2010)).

CAPTION

Figure 1 Constant-ψ contours on the R-Z plane for $S=2.65\times10^7$, where R=0 corresponds to the major radius of the original magnetic axis, and Z is the coordinate along the vertical direction, normalized to the plasma minor radius a. (a) At t=12008 τ_A, a small secondary island forms on the left hand side of the core region. (b) At t=12527 τ_A, the original core region is squeezed into a thin layer by the 1/1 and the secondary island, and this layer is then broken up, leading to the third island on the upper and lower left corner. (c) At t=12622 τ_A, the third island moves outwards and reconnects there. (d) At t=23890 τ_A, during the phase when both the m/n=1/1 and the secondary island slowly change in time.

Figure 2 Plasma current density contours shortly after the breaking up of the current sheet for $S=2.65\times10^7$ (a), 2.65×10^8 (b) and 2.65×10^9 (c). (d) shows the plasma current density contours at t=17325 τ_A in the later nonlinear phase for $S=2.65\times10^7$.

Figure 3 (a) The time evolution of the helical flux at the x- point, ψ_x, (solid curve with circles) and the o-point, ψ_o, (dotted curve) of the m/n=1/1 island for $S=2.65\times10^6$, 2.65×10^7, 2.65×10^8, and 10^9. The dashed curves are for the helical flux at the o-point of the secondary island. (b) Same as (a) except that the helical flux at the x- point (marked as x-3rd) and the o-point (marked as o-3rd) of the third island is shown for $S=2.65\times10^7$.

Figure 4 The maximum or saturated radial island width (normalized to plasma minor radius) versus S. The curve with circles (squares) corresponds to the m/n=1/1 (secondary) island.

Figure 5 Reconnection time (normalized to τ_A) versus S. The curve with circles represents the m/n=1/1 island growth time from the width w=0.1a up to the maximum or saturated island width. The straight lines with triangles is calculated according to Kadomtsev's model.

Figure 1

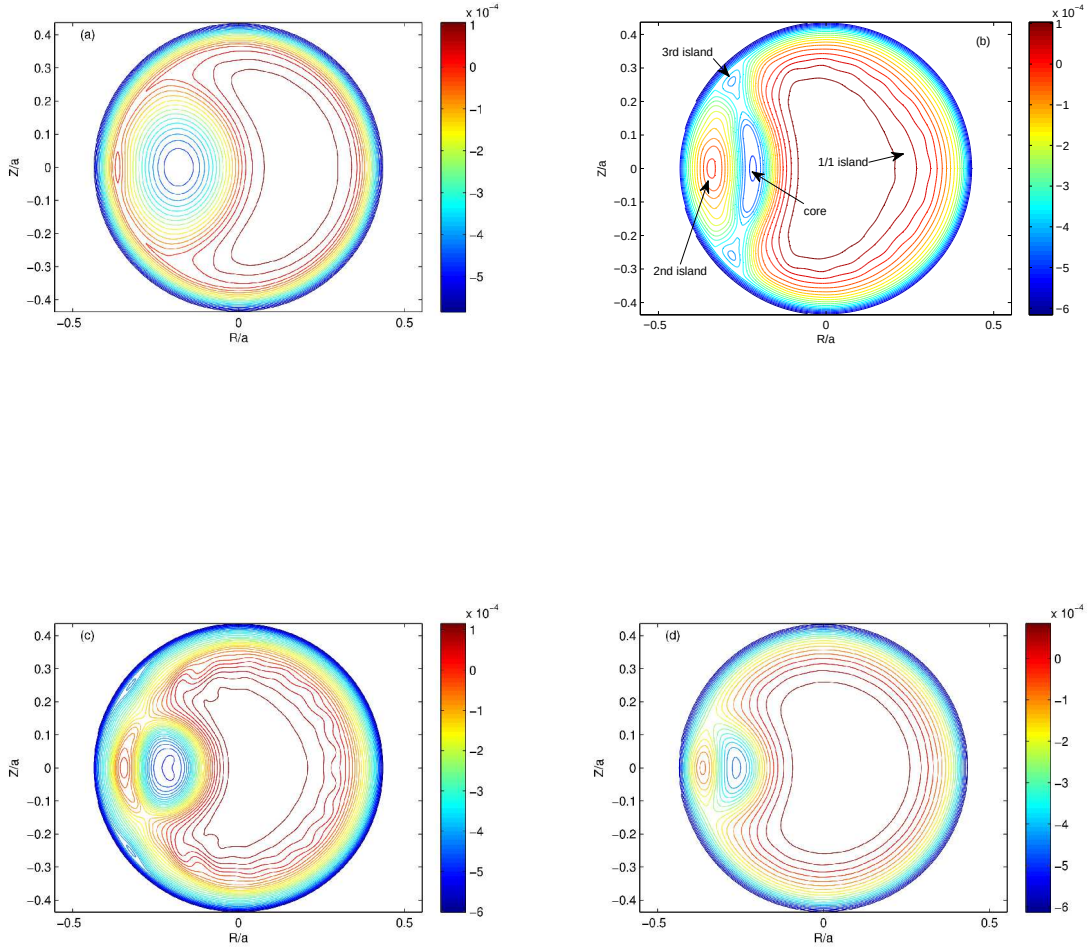

Figure 2

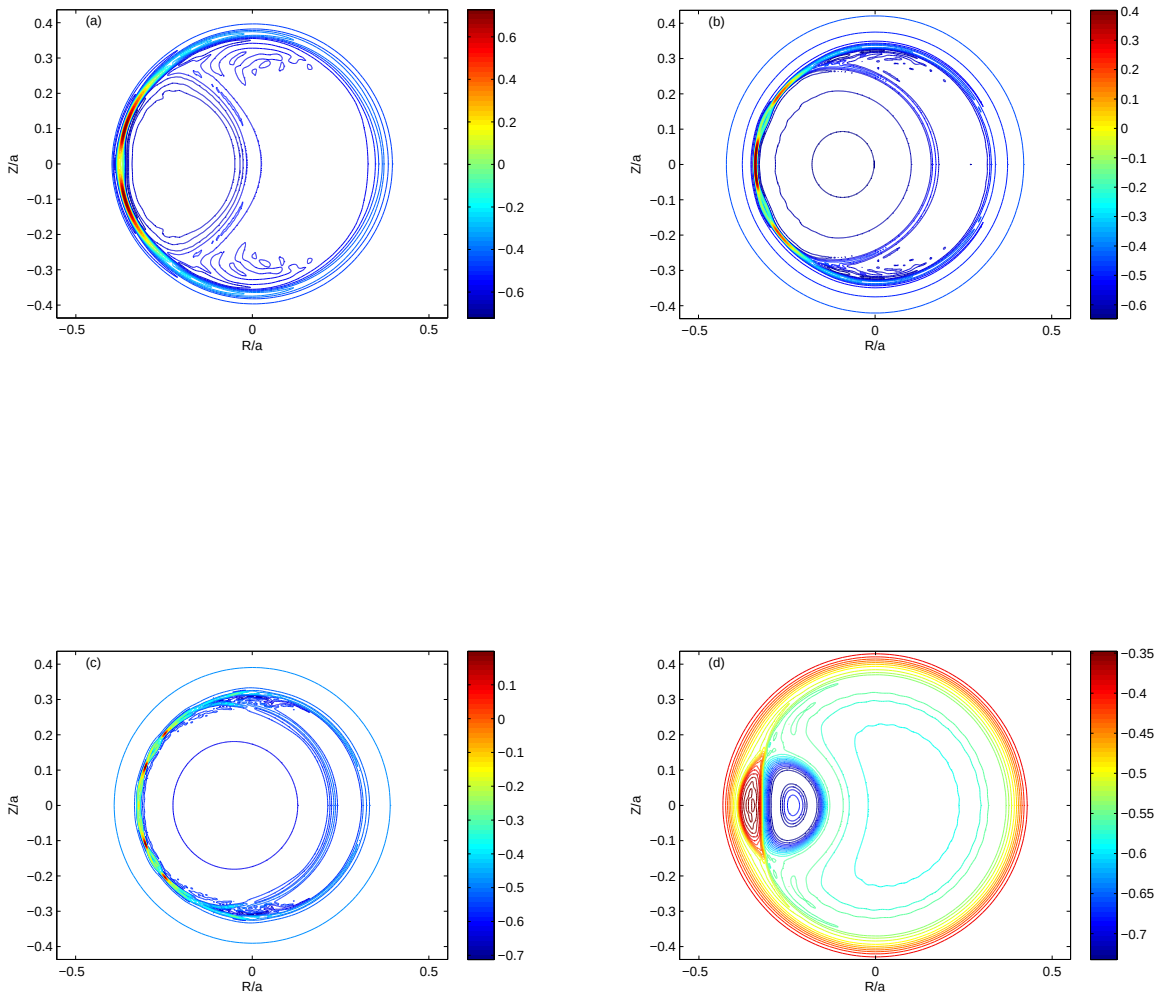

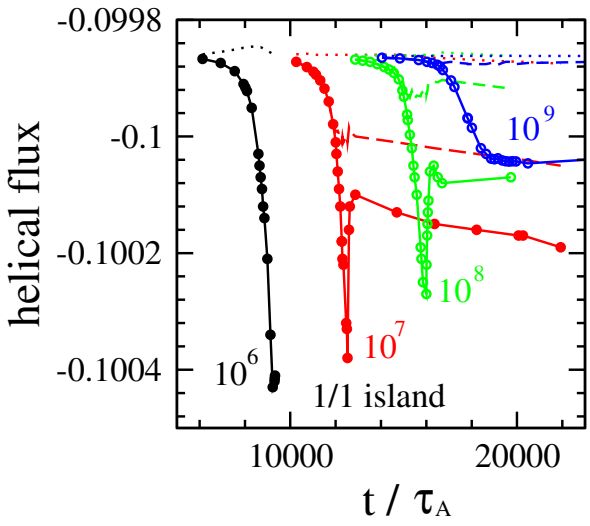
-0.0998
-0.1
-0.1002
-0.1004
helical flux
10000
20000
t / τA
10^6
10^7
10^8
10^9
1/1 island

Figure 3a

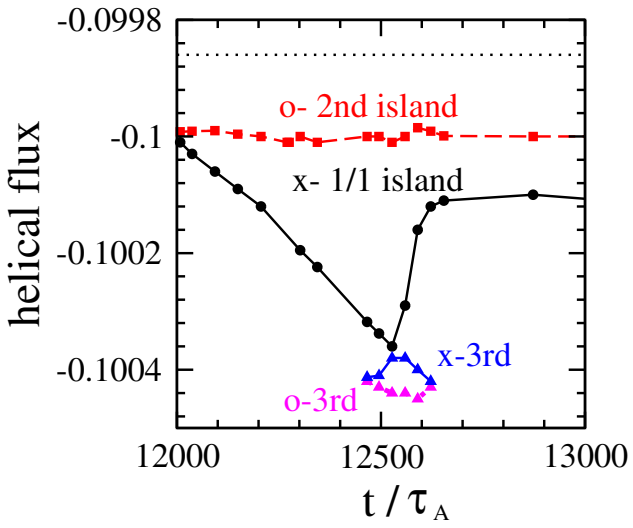
-0.0998
-0.1
-0.1002
-0.1004
helical flux
o- 2nd island
x- 1/1 island
x-3rd
o-3rd
12000
12500
13000
t / τ A

Figure 3b

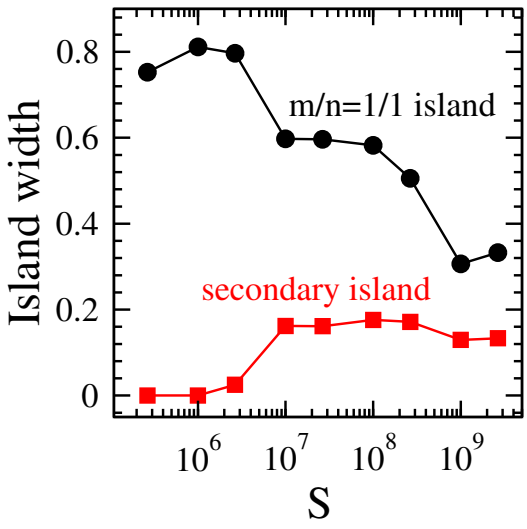
Island width
0.8
0.6
0.4
0.2
0
m/n=1/1 island
secondary island
10^6
10^7
10^8
10^9
S

Figure 4

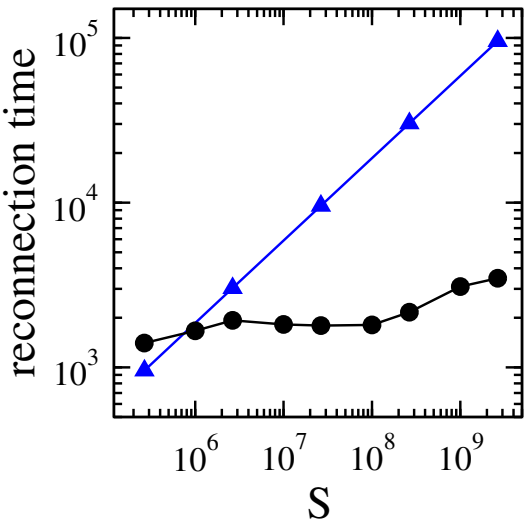

Figure 5